THE JOURNAL OF PHYSICAL CHEMISTRY B

Article

pubs.acs.org/JPCB

Understanding the Ion Jelly Conductivity Mechanism

T. Carvalho,[†] V. Augusto,[†] A. R. Brás,[†,‡] N. M. T. Lourenço,[§] C. A. M. Afonso,[∥,⊥] S. Barreiros,[†] N. T. Correia,[†,⊗] P. Vidinha,[†] E. J. Cabrita,[†] C. J. Dias,[○] M. Dionísio,*[,†] and B. Roling[#]

[†]REQUIMTE, Departamento de Química, Faculdade de Ciências e Tecnologia da Universidade Nova de Lisboa, 2829-516 Caparica, Portugal

[‡]Jülich Centre for Neutron Science (JCNS-1) & Institute for Complex Systems (ICS-1), Forschungszentrum Jülich, 52425 Jülich, Germany

[§]IBB-Institute for Biotechnology and Bioengineering, Centre for Biological and Chemical Engineering, Instituto Superior Técnico, Av. Rovisco Pais, 1049-001 Lisboa, Portugal

[∥]CQFM, Centro de Química-Física Molecular, IN-Institute of Nanosciences and Nanotechnology, Instituto Superior Técnico, 1049-001 Lisboa, Portugal

[⊥]iMed. UL, Faculdade de Farmácia da Universidade de Lisboa, Av. Prof. Gama Pinto, 1640-003 Lisboa, Portugal

[⊗]Unité Matériaux et Transformation (UMET), UMR CNRS 8207, UFR de Physique, BAT P5, Université Lille 1, 59655 Villeneuve d'Ascq, France

[○]CENIMAT/I3N, Departamento de Ciências dos Materiais, Faculdade de Ciências e Tecnologia da Universidade Nova de Lisboa, 2829-516 Caparica, Portugal

[#]Fachbereich Chemie, Philipps-Universität Marburg, Hans-Meerwein Strasse, D-35032 Marburg, Germany

ABSTRACT: The properties of the light flexible device, ion jelly, which combines gelatin with an ionic liquid (IL) were recently reported being promising to develop safe and highly conductive electrolytes. This article aims for the understanding of the ion jelly conductive mechanism using dielectric relaxation spectroscopy (DRS) in the frequency range 10^{-1}–10^{6} Hz; the study was complemented with differential scanning calorimetry (DSC) and pulsed field gradient nuclear magnetic resonance (PFG NMR) spectroscopy. The room temperature ionic liquid 1-butyl-3-methylimmidazolium dicyanamide (BMIMDCA) used as received (1.9% w/w water content) and with 6.6% (w/w) of water content and two ion jellies with two different ratios BMIMDCA/gelatin/water % (w/w), IJ1 (41.1/46.7/12.2) and IJ3 (67.8/25.6/6.6), have been characterized. A glass transition was detected by DSC for all materials allowing for classifying them as glass formers. For the ionic liquid, it was observed that the glass transition temperature decreases with the increase of water content. While in subsequent calorimetric runs crystallization was observed for BMIMDCA with negligible water content, no crystallization was detected for any of the ion jelly materials upon themal cycling. To the dielectric spectra of all tested materials, both dipolar relaxation and conductivity contribute; at the lowest frequencies, electrode and interfacial polarization highly dominate. Conductivity, which manifests much more intensity relative to dipolar reorientations, strongly evidences subdiffusive ion dynamics at high frequencies. From dielectric measures, transport properties as mobility and diffusion coefficients were extracted. Data treatment was carried out in order to deconvolute the average diffusion coefficients estimated from dielectric data in its individual contributions of cations (D_+) and anions (D_-). The D_+ values thus obtained for IJ3, the ion jelly with the highest IL/gelatin ratio, cover a large temperature range up to room temperature and revealed excellent agreement with direct measurements from PFG NMR, obeying to the same VFT equation. For $BMIMDCA_{6.6\%water}$, which has the same water amount as IJ3, the diffusion coefficients were only estimated from DRS measurements over a limited temperature range; however, a single VFT equation describes both DRS and PFG NMR data. Moreover, it was found that the diffusion coefficients and mobility are similar for the ionic liquid and IJ3, which points to a role of both water and gelatin weakening the contact ion pair, facilitating the translational motion of ions and promoting its dissociation; nevertheless, it is conceivable the existence of a critical composition of gelatin that leads to those properties. The VFT temperature dependence observed for the conductivity was found to be determined by a similar dependence of the mobility. Both conductivity and segmental motion revealed to be correlated as inferred by the relatively low values of the decoupling indexes. The obtained results show that ion jelly could be in fact a very promising material to design novel electrolytes for different electrochemical devices, having a performance close to the IL but presenting an additional stability regarding electrical measurements and resistance against crystallization relative to the bulk ionic liquid.

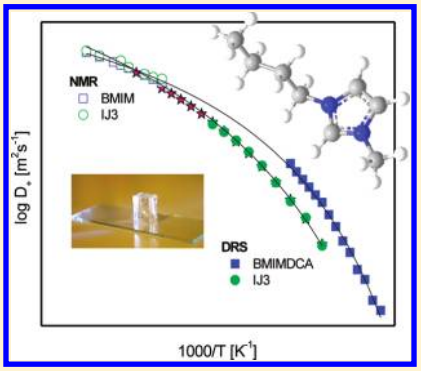

1. INTRODUCTION

Ionic liquids (ILs) are probably one of the most studied chemical compounds in the past decade. This is particularly motivated by

Received: November 11, 2011
Revised: January 24, 2012
Published: February 27, 2012

ILs unique physical−chemical properties that enable their application on a broad range of scientific fields. ILs are comprised entirely by ions and most of them exhibit a negligible vapor pressure, ionic conductivity, and a high thermal, chemical, and electrochemical stability.[1−3]

Nevertheless, the tailor-made design of ILs is probably the most fascinating and creative domain on IL research. The design, however, is imperative to evaluate the fundamental physical−chemical properties before trying to evolve a given IL structure for a particular application. For instance, the type of molecular interaction between cation and anion is determinant for physical−chemical properties such as melting temperature, glass transition temperature, T_g, or conductivity.[4,5]

This set of properties has attracted their application as novel electrolytes for different electrochemical devices, such as dye synthesized solar cells, double layer capacitors, fuel cells, electrochemical windows, and, of course, lithium secondary batteries.[1,3]

In fact, the actual trend in electrochemical devices point to ILs as the most promising approach to develop safe and highly conductive electrolytes. Nevertheless, the large scale fabrication of the above electrochemical devices is following the printing trend due to large scale production impositions. To address this issue, different authors have tried to develop solid/polymeric/composite-based ionic liquids.[6−9]In fact, some of these systems have been very competitive in terms of ionic conductivity.[7,8]

One of the most simple and efficient approaches is based on gelation, which is a simple method that allows a good compromise between the retention of the IL and its fluidity inside the polymeric network. This strategy is quite different from the traditional solid polymer electrolytes that results either from the doping of a given polymer matrix with an IL or by the introduction of polymerizable groups on ILs structures. These so-called ion gels are in such a way simpler than solid polymer electrolytes and exhibit improved conductivities. For instance, McFarlane and co-workers[7] have shown the potential of an ion gel formed by gelation of poly(styrene-block-ethylene oxide-block-styrene) (SOS) triblock copolymer in 1-butyl-3-methylimidazolium hexafluorophosphate. This system has shown interesting conductivity values at room temperature (above 10^{-3} S cm^{-1}).

This field of research has been developed in order to create IL-based materials that can work as electrolytes in different electrochemical devices and be used either as printer substrates or printable inks.

Following this trend, we recently reported ion jelly (IJ), a light flexible electrolyte that results from the combination of gelatin with an IL. This allows the production of gelatin gels that are extremely versatile conductive materials that can be molded into different shapes, using several techniques, and can be adapted to multiple surfaces. Moreover, on cooling, ion jelly can undergo a liquid-gel transition near room temperature (near 308 K), which makes a promising solution to develop electrolyte inks for printed electrochemical devices (PED).[10]

The evaluation of basic thermophysical properties is vital to the design of IJs and to conceive new applications.

For that propose, it is essential to understand the physicochemical behavior of ILs in an ion jelly matrix. To accomplish this goal, we have performed a dielectric relaxation spectroscopy characterization (DRS).

Basically, DRS spectra reproduce the set of molecular motions of all dipolar species present in the media. In ionic liquids, these motions are highly correlated with the multiplicity of interaction between the different charged species present in the media, which makes it impossible to address a specific motion to a well-defined dipole. In fact, on ILs, the molecular motions reflect the kinetics of the network rearrangement.[11,12] However, the ion jelly network is settled by the interaction between two polyelectrolyte molecules (gelatin and IL) creating in such way a complex network with multiple interaction sites that can lead to a great variety of dipolar aggregates. Moreover, since these materials have some degree of hydration, the role of water needs also to be evaluated. Thus, a comprehensive and detailed analysis of IL relaxation behavior inside a hydrated gelatin matrix can result in important data about the crucial mechanisms implicated on the ion jelly conductivity.

The ion jelly system chosen for this study is based on 1-butyl-3-methyl imidazoliumdicyanamide (BMIMDCA). The dicyanamide (DCA) compounds are liquid at room temperature and characterized by their low viscosity, water miscibility, and high thermo (over 373 K) and electrochemical stability (over 3.5 V).[11,12] Moreover, the dicyanamide ion is an anionic bridge ligand that has Lewis base attributes, which makes it particularly attractive to synthesize ionic liquids with very specific properties. Compared to common anions such as PF_6 or BF_4, DCA has a permanent dipole and thus facilitates the research of IL dynamics through dielectric spectroscopy.[12,13]

On the basis of the analysis of the thermal behavior, charge transporters, ion mobility, and conductivity, we are able to obtain useful information that could illustrate the impact of gelatin on IL physicochemical properties, which are ultimately implicated on ion jelly conductivity and consequently on its application to PEDs.

2. EXPERIMENTAL SECTION

2.1. Materials. The room temperature ionic liquid 1-butyl-3-methylimmidazolium (BMIM-cation) dicyanamide (DCA-anion), $C_{10}H_{15}N_5$ (MW, 205.26; density$_{298\ K}$[14]= 1.058 g cm^{-3}) was provided by Iolitec, ref 448245−52−1, purity >98%. Gelatin was purchased from Panreac ref 403 902. Both materials were used as received.

2.1.1. Ion Jelly Preparation. To prepare IJ1 (IJ3), 100 μL (300 μL) of BMIMDCA was heated to 313 K under magnetic stirring, followed by the addition of 120 mg of gelatin; the designation 1 and 3 in the ion jelly materials gives the ratio of BMIMDCA/gelatin in the starting mixture. In order to obtain a homogeneous solution, 206 μL (75 μL) of water was added dropwise. The mixtures were kept stirring at 313 K until the gelatin was completely solubilized (approximately 15 min). The solutions were then spread over a glass surface in order to form thin films. Jellification occurred at room temperature.

To have a blank for comparison on the influence of gelatin, a gelatin film was prepared by adding 120 mg of gelatin to 1020 μL of water at 313 K under magnetic stirring in order to obtain a homogeneous solution.The solution was also spread over a glass surface at room temperature to form a film.

Karl Fischer titration was used to determine the water content in each final material as IJ1-12.2%, IJ3-6.6%, and BMIMDCA-1.9% as received (w/w); the water content in the gelatin film was determined to be 22% (w/w). No lower water amounts were possible to achieve gelatin films; otherwise, no self-supported films are obtained.

To evaluate the influence of water in conductive and transport properties, water was added to the as received BMIMDCA until a final content of 6.6% (w/w) was achieved

dx.doi.org/10.1021/jp2108768 | J. Phys. Chem. B 2012, 116, 2664−2676

(quantified by Karl Fischer titration) having the same water amount as IJ3; the two BMIMDCA materials will be designated hereafter as $BMIMDCA_{1.9\%water}$ and $BMIMDCA_{6.6\%water}$.

The final composition of the ion jelly materials is thus IJ1-IL/gelatin/water = 41.1/46.7/12.2% (w/w) and IJ3-IL/gelatin/water = 67.8/25.6/6.6% (w/w).

2.2. Techniques. *2.2.1. Differential Scanning Calorimetry.* DSC measurements were performed in a SETARAM DSC 131 calorimeter. The melting heat of indium was used for calibrating heat flow. Samples ~26 mg (39 mg of $BMIMDCA_{6,6\%water}$) were placed in open aluminum pans; an empty aluminum pan was used as reference. Dry high purity N_2 gas was purged through the samples during the measurements. The two ion jellies, $BMIMDCA_{1.9\%water}$, $BMIMDCA_{6.6\%water}$, and gelatin were analyzed. Thermograms were collected, after a previous cooling run down to 123 K, upon heating to 363 K at a rate of 20 K min^{-1}. This relatively high heating rate was chosen to enhance the heat capacity step in the ion jelly materials, mainly in IJ1 for which the jump is quite broad.

2.2.2. Dielectric Relaxation Spectroscopy. For the dielectric spectroscopy measurements, films were cut into disks of about 10 mm in diameter. The films thickness was 0.5 and 0.7 mm, respectively, for IJ1 and IJ3; no thinner films were possible to obtain being the thickness limited by the formation of a self-supported gelatin film. For the BMIMDCA samples, two silica spacers of 0.05 mm thickness were used. The samples were placed between two gold plated electrodes (10 mm diameter) in a parallel plate capacitor, BDS 1200. The sample cell was mounted on a cryostat, BDS 1100, and exposed to a heated gas stream being evaporated from liquid nitrogen in a Dewar. The temperature control was assured by the Quatro Cryosystem and performed within ±0.5 K (all modules supplied by Novocontrol). Measurements were carried out using an Alpha-N analyzer also from Novocontrol GmbH, covering a frequency range from 10^{-1} Hz to 1 MHz. After a first cooling ramp from room temperature to 163 K, isothermal spectra were collected in steps of 5 K up to 248 K (IJ1) and 303 K (IJ3). Both BMIMDCA were isothermally measured from 143 K up to 213 K; from 143 to 153 K in steps of 5 K and from 153 to 213 K in steps of 2 K.

The dielectric relaxation data obtained were deconvoluted using a sum of the model function introduced by Havriliak–Negami[15]

$$\varepsilon^*(\omega) = \varepsilon_\infty + \sum_j \frac{\Delta\varepsilon_j}{[1 + (i\omega\tau_j)^{\alpha_{HNj}}]^{\beta_{HNj}}} \quad (1)$$

where j is the number of relaxation processes, $\Delta\varepsilon = \varepsilon_s - \varepsilon_\infty$ is the dielectric strength, i.e., the difference between the real permittivity values at, respectively, the low and high frequency limits, τ_{HN} is the relaxation time, and α_{HN} and β_{HN} are the shape parameters ($0 < \alpha_{HN} < 1$; $0 < \alpha_{HN}\beta_{HN} < 1$). Since data are strongly influenced by the low frequency conductivity contribution, an additional term $i\sigma/\omega^c\varepsilon_o$ was added to the dielectric loss, where ε_0 is the vacuum permittivity; σ and c are fitting parameters: σ is related to the dc conductivity of the sample, and the parameter c ($0 < c \leq 1$) reflects conductivity of ions for $c = 1$ and for $c < 1$ interfacial polarizations, including electrode polarization.

2.2.3. Nuclear Magnetic Resonance. NMR spectra were recorded on a Bruker Avance III 400 spectrometer, operating at 400.15 MHz, equipped with pulse gradient units, capable of producing magnetic field pulsed gradients in the z direction of 0.54 T m^{-1}. Diffusion measurements were performed using the stimulated echo sequence using bipolar sine gradient pulses and eddy current delay before the detection.[16] The signal attenuation is given by

$$S = S_0 \exp\left(-\gamma^2 g^2 D\delta^2\left(\Delta - \frac{2\delta}{3} - \frac{\tau_g}{2}\right)\right)$$

where D denotes the self-diffusion coefficient, γ the gyromagnetic ratio, δ the gradient pulse width, Δ the diffusion time, τ_g the gradient recovery delay, and g the gradient strength corrected according to the shape of the gradient pulse.

Before all NMR experiments, the temperature was equilibrated and maintained constant within ±0.1 K, as measured using the spectrometer thermocouple system. Experiments were performed at 298.15 K, 288.15 K, 278.15 K, 273.15 K, 268.15 K, 258.15 K, 253.15 K, and 248.15 K.

The spectra were recorded in 5 mm NMR tubes with an air flow of 535 L h^{-1}. Typically, in each experiment, a number of 32 spectra of 32 K data points were collected, with values for the duration of the magnetic field pulse gradients (δ) of 2.5 to 3.5 ms, diffusion times (Δ) of 400 to 2000 ms, and an eddy current delay set to 5 ms, the gradient recovery time (τ_g) was 200 μs. The sine shaped pulsed gradient (g) was incremented from 5 to 95% of the maximum gradient strength in a linear ramp. The spectra were first processed in the F2 dimension by standard Fourier transform and baseline correction with the Bruker Topspin software package (version 2.1). The diffusion coefficients are calculated by exponential fitting of the data belonging to individual columns of the 2D matrix. The diffusion coefficients (D) were obtained by measuring the signal intensity at more than one place in the spectra. At least two different measurements were done for the determination of each diffusion coefficient.

3. RESULTS AND DISCUSSION

3.1. Thermal Characterization. To obtain a proper understanding of the transport properties of IJs and BMIMDCA, the thermal transitions were first investigated by DSC. The respective thermograms, recorded in heating mode, are presented in Figure 1.

For $BMIMDCA_{1.9\%water}$, $BMIMDCA_{6.6\%water}$, and IJ3, it is clear the heat flow jump, which is the characteristic signature of the glass to supercooled liquid transition; although not so clear, the same transition is also observed for IJ1. Therefore, all the materials tested in this work are classified as glass formers. In this temperature range, no transition was detected for gelatin.

The width of the transition is higher for both ion jelly materials, in particular for IJ1, which covers an extremely wide temperature range, relative to BMIMDCA either with 1.9 or 6.6% of water. As a result, the glass transition temperature determined from the onset of the calorimetric signal will be taken for comparison being 174.2 K (−99.0 °C), 169.8 K (−100.5 °C), 174.4 K (−98.8 °C), and 203.9 K (−69.2 °C) for, respectively, $BMIMDCA_{1.9\%water}$, $BMIMDCA_{6.6\%water}$, IJ3, and IJ1 (see Table 1). The values extracted from the midpoint and endset are also included in Table 1, as well as the heat capacity jump. While the onset of the glass transition detected for IJ3 occurs near to the onset of the bulk ionic liquid, the temperature of the glass transition increases significantly in IJ1. This will be confirmed later by DRS. For the ionic liquid, it is observed a decrease of the glass transition with the water

dx.doi.org/10.1021/jp2108768 | J. Phys. Chem. B 2012, 116, 2664–2676

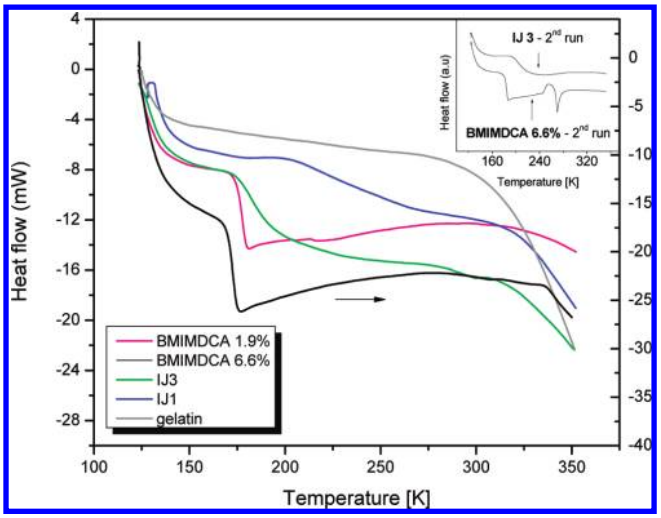

Figure 1. DSC scans obtained in heating mode at 20 K min^{-1} for $BMIMDCA_{1.9\%water}$, $BMIMDCA_{6.6\%water}$, and both ion jellies showing the heat flow jump at the glass transition; in the studied temperature range, no transitions are detected for gelatin. The inset shows the second heating scan for $BMIMDCA_{6.6\%water}$ and IJ3, where cold crystallization and melt are observed for the IL and avoided for the ion jelly (see text).

Table 1. Glass Transition Temperatures Taken at the Onset (on), Midpoint (mid), and Endset (end) of the Heat Flow Jump for Both BMIMDCA and Both Ion Jellies, Obtained during a First Heating Ramp at 20 K/min, and Heat Capacity Associated with the Glass Transition

system	$T_{g,on}$ (K)	$T_{g,mid}$ (K)	$T_{g,end}$ (K)	ΔC_p(J g^{-1} K^{-1})
$BMIMDCA_{1.9\%water}$	174.2	177.6	179.7	0.68
$BMIMDCA_{6.6\%water}$	169.8	172.5	177.8	0.72
IJ3	174.4	181.8	193.3	0.47
IJ1	203.9	220.6	256.0	0.30

content. This is consistent with the data provided by Fredlake et al.[14] for BMIMDCA with lower water content (0.515%) for which a higher T_g value is reported: 183 K (−90 °C) taken at the midpoint; in this work, the $T_g$values taken at the midpoint were estimated as, respectively, 177.6 K (−95.6 °C) and 172.5 K (−100.65 °C) for $BMIMDCA_{1.9\%water}$ and $BMIMDCA_{6.6\%water}$. Therefore, a plasticizing effect of water at these relative low water contents can be inferred. The shift of the position of the glass transition toward lower temperatures was also observed for another IL, 1-ethyl-3-methylimidazolium acetate, for water contents from 0 up to 40% w/w.[17]

In addition to the glass transition, Fredlake et al.[14] report the occurrence of cold crystallization at 244 K (−29 °C) followed by melting at 267 K (−6 °C) for BMIMDCA. This was investigated here for both BMIMDCA, and indeed, cold crystallization of the supercooled liquid and subsequent melt are detected at temperatures close to those reported in ref 14 but only in a second heating run (see the illustrative thermogram for $BMIMDCA_{6.6\%water}$ in the inset of Figure 1). It is worth noting that prior to the second heating run during which crystallization was observed, the sample was heated up to 363 K in the first heating scan and kept 5 min at this temperature. This assures the water removal, which seems to be a condition to occur further crystallization. In the second heating scan, the glass transition temperature increased to 184.6 K for both $BMIMDCA_{6.6\%water}$ and $BMIMDCA_{1.9\%water}$ (taken at the midpoint), confirming the shift to higher temperatures upon dehydration, and the water content remaining in both samples is similar and probably negligible (at least below 0.5% according to the previous discussion). Moreover, no crystallization was observed in subsequent runs for both ion jellies (see the second heating scan for IJ3 in the inset of Figure 1). This can be taken as an indication that, upon thermal treatments, the supramolecular structure of gelatin stabilizes to some extent (i) the disordered amorphous state of the IL and (ii) the water retention. This can be seen as a plus concerning the potential apllications and performance of these materials.

The first scan is the one taken for all samples since it reproduces the conditions followed in the dielectric measurements.

In summary, from the calorimetric characterization, we conclude that all ionic liquid-based materials here investigated are glass formers. For the bulk ionic liquid, the glass transition temperature decreases upon hydration. The ion jelly material with the higher amount of ionic liquid (IJ3) has a glass transition temperature (measured in the first heating run) close to that of both BMIMDCA structures. Advantageously, both ion jellies did not undergo further crystallization after water removal contrary to which is observed for BMIMDCA with either 1.9 or 6.6% water content. The ion jelly with the lower IL content, although having the highest water amount (12%), presents the higher glass transition temperature, probably due to the high gelatin:BMIMDCA ratio.

3.2. Dielectric Characterization. *3.2.1. Conductivity.* Figure 2 shows the real (a−d) and imaginary (e−h) components of the complex conductivity, $\sigma^*(\omega) = \sigma'(\omega) + i\sigma''(\omega)$, from 10^{-1} to 10^6 Hz covering different temperature ranges for each material: $BMIMDCA_{1.9\%water}$, $BMIMDCA_{6.6\%water}$, IJ3, and IJ1 from top to bottom. The insets show the respective components of the dielectric complex function $\varepsilon^*(\omega) = \varepsilon'(\omega) - i\varepsilon''(\omega)$ associated with reorientational motions of dipoles. The relationship between both is given by[18] $\sigma^*(\omega) = i\omega\varepsilon_0\varepsilon^*(\omega)$. As it becomes clear from the permittivity and loss curves, conductivity strongly affects the dipolar spectra mainly at the low frequency side and at the highest temperatures. This conductivity contribution can be analyzed to extract information on the charge transport mechanism for each material, which will be carried out in the next section.

To evaluate the influence of gelatin itself in the ion jelly conductivity, a film of gelatin with 22% of water was also measured at 298 K; this was the minimal water content that allowed preparing self-supported gelatin films. Figure 3 shows the real conductivity for this material. It is evident that the dielectric response for $gelatin_{22\%water}$ is significantly lower relative to any of the tested materials of either IL or IJ. Even at the highest frequencies, the real conductivity of $gelatin_{22\%water}$ is around 4 decades inferior to that of IJ3; at the lowest frequencies, the response differs around 8 decades! The role of water will be analyzed in the end of section 3.2.2.

It is worthy to mention that while the dielectric measurements for the ionic liquid (either with 1.9 or 6.6% water) were affected by electrical anomalies at temperatures close to room temperatures and at the highest frequencies (that persist even reducing the length of the BNC connecting cables), no such instabilities were felt while measuring the ion jelly materials. This can be taken as another advantage of the performance of these devices.

dx.doi.org/10.1021/jp2108768 | J. Phys. Chem. B 2012, 116, 2664−2676

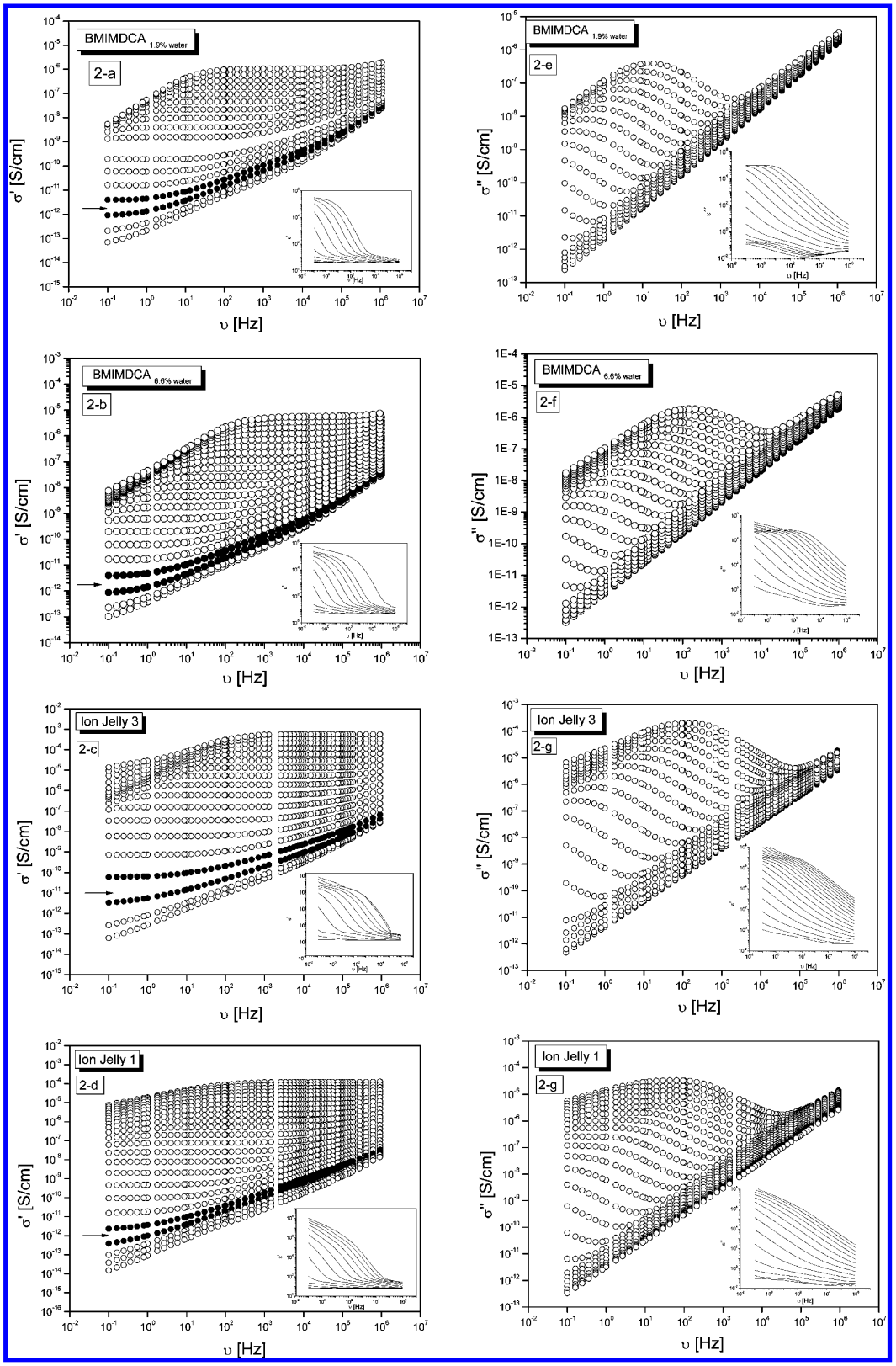

Figure 2. Complex conductivity measured at different temperatures of $BMIMDCA_{1.9\%water}$ and $BMIMDCA_{6.6\%water}$ (in steps of 2 K from 163 to 213 K) and ion jelly (in steps of 5 K starting at 163K (IJ3) and 188K(IJ1)): (a–d) real, σ', and (d–g) imaginary, σ'', components; the onset of the calorimetric T_g occurs at a temperature in between the isotherms represented by filled symbols (indicated by the arrow). The insets display the respective real ε' (a–d) and imaginary ε'' (e–h) parts of the complex dielectric function.

The plot of the real part of the complex conductivity (Figure 2a–d) presents a profile similar to the one found for a variety of quite different materials:[19−21] a plateau at low frequencies that bends off at some critical frequency into a dispersive regime, with a strong increase of the conductivity with increasing frequency following a power

dx.doi.org/10.1021/jp2108768 | J. Phys. Chem. B 2012, 116, 2664–2676

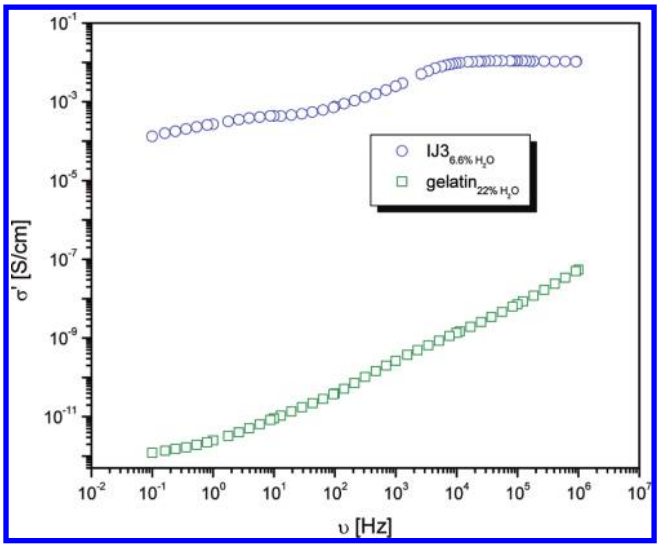

Figure 3. Frequency dependence of real conductivity at 298 K for IJ3 (which has 6.6% (w/w) water content) compared with a blank of a gelatin film with 22% (w/w) of water (see section 2).

law dependence (a.c. conductivity) as proposed by Jonscher[22]

$$\sigma'(\omega) = \sigma_0\left[1 + \left(\frac{\omega}{\omega_{cross}}\right)^s\right] \quad (2)$$

Where s $(0.5 \leq s \leq 1)$[18] is a material- and temperature-dependent parameter, allowing to obtain ω_{cross}.

The crossover frequency defines the transition from a diffusive dynamics of charge transport ($\omega < \omega_{cross}$) to a subdiffusive regime ($\omega > \omega_{cross}$): the former is a long-time dynamics characterized by random walks resulting in long-range ion transport, whereas the subdiffusive regime is a short-time dynamics characterized by back-and-forth motion over limited ranges.[23] At the lowest temperatures, the regime is always subdiffusive, and no crossover is observed. The emergence of a ω_{cross} in the real conductivity spectrum provides a way to get a rough estimate of the glass transition temperature as found for both BMIMDCA materials and IJ3 from which an unequivocal calorimetric determination of T_g was possible (the arrow in Figure 2a–d indicates the two temperatures that lie immediately below and above the onset of the T_g detected by DSC). In the case of IJ1, an identical behavior is observed between the isotherms collected at 203 K and 208 K giving further evidence that the glass transition temperature is closer to the value hardly estimated from DSC measurements ($T_{g,on}$ = 204 K).

The plateau region corresponds to a linear dependence of slope 1 in the plots of $\log(\varepsilon''(\omega))$ and gives the value of σ_0, the conductivity in the dc limit. At the highest temperatures in each collection of $\sigma'(\omega)$ spectra, instead of an extended plateau in the conductivity plot in the low frequency region, a decrease is observed, due to electrode polarization as found in similar materials.[24] This means that ionic conduction becomes blocked, i.e., ions accumulate in the sample/electrode interface without discharging. In the same frequency region, the loss curves ($\varepsilon''(\omega)$) present a linear dependence with a slope <1, and the real permittivity ($\varepsilon'(\omega)$) exhibits a tail with several orders of magnitude higher than the values measured at the lowest temperatures and highest frequencies. Additionally, when electrode polarization occurs, a peak is observed in the imaginary part of the conductivity, $\sigma''(\omega)$, as depicted in Figure 2e–h. A more detailed analysis of $\varepsilon'(\omega)$ and $\sigma''(\omega)$ will be provided in section 3.2.3.

Equation 2 was fitted to the real part of conductivity to obtain ω_{cross} and σ_0; the latter compares very well with values taken from the plateau region in each isotherm. Figure 4 shows

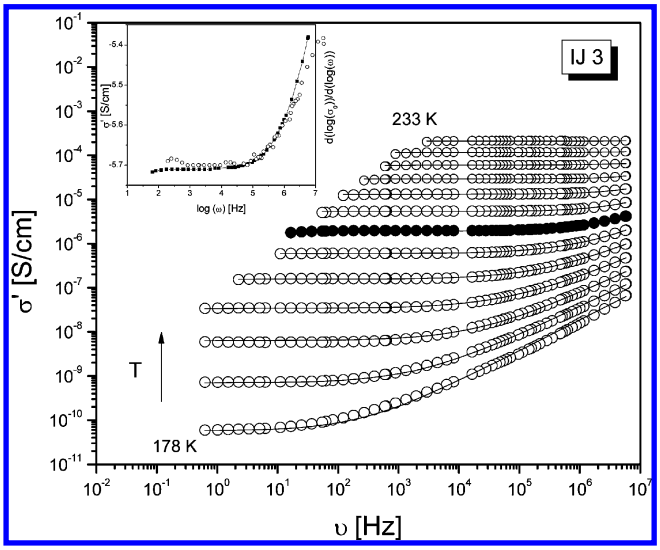

Figure 4. Real part of conductivity for IJ3 from 178 to 233 K in steps of 5 K. The solid lines are the obtained fits by the Jonscher law (eq 2). Data collected at 208 K are plotted in full circles being the same spectrum presented in the inset together with the respective derivative $d(\log \sigma'(\omega))/d(\log(\omega))$ (open circles); the continuous increase of the derivative value with the frequency increasing confirms the subdiffusive dynamics (see text).

for IJ3 the obtained fit as solid lines at temperatures for which data are not influenced by electrode polarization (an effect that is not taken into account in the proposed law). The curve taken at 208 K is plotted in full symbols being the same presented in the inset that also includes its respective derivative plot $d(\log \sigma'(\omega))/d(\log(\omega))$ (open circles). This is a way to verify if ion transport at short times (high frequency side of spectrum) is governed by subdiffusive dynamics. In fact, if dipolar relaxation dominates, a different profile for the a.c. contribution would be obtained.[25,26] Moreover, subdiffusive bulk ion dynamics usually leads to an apparent slope $d(\log \sigma'(\omega))/d(\log(\omega))$, which increases continuously with increasing frequency. In contrast, reorientational motions of dipoles lead to a ε'' peak, which implies that in the low-frequency flank of the peak, the slope $d(\log \sigma'(\omega))/d(\log(\omega))$ is larger than unity, and in the high-frequency flank, it is smaller than unity. So, in the case of reorientional motions, one does not expect a continuous increase of the slope with increasing frequency as we obtained. Therefore, there is strong evidence that subdiffusive dynamics dominate at short times allowing to extract transport properties (section 3.2.2).

The temperature dependence of the σ_0 values is plotted in Figure 5 for the four materials. The empirical VFT equation[27−29] was fitted to the conductivity data, which usually describes the temperature dependence of the dynamic glass transition relaxation time (eq 3a) and the electrical conductivity (eq 3b)

dx.doi.org/10.1021/jp2108768 | J. Phys. Chem. B 2012, 116, 2664−2676

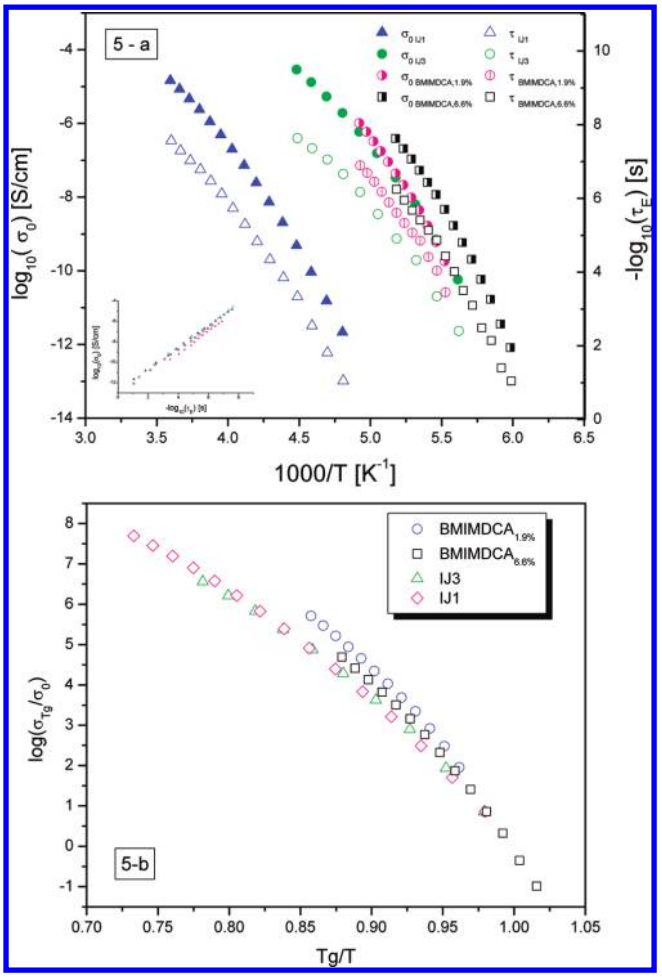

Figure 5. (a) Temperature dependence of the dc conductivity, σ_0, and of the relaxation time, τ_e, taken from the crossover frequency. The correlation between both is displayed in the inset (BNN plot) for which a slope near 1 and a $r^2 = 0.99$ was found: $\log(\sigma_0) = (1.06 \pm 0.02)\log(\tau_e) - (12.95 \pm 0.09)$. (b) Temperature dependence of conductivity normalized for the value measured at the calorimetric glass transition temperature (σ_{Tg}); the temperature axis is scaled to the glass transition temperature, T_g.

of supercooled liquids, including ionic liquids,[6,13,26,30−32] quite well

$$\tau(T) = \tau_\infty \exp\left(\frac{B}{T - T_0}\right) \quad (3a)$$

$$\sigma_0(T) = \sigma_\infty \exp\left(-\frac{B}{T - T_0}\right) \quad (3b)$$

where τ_∞ and σ_∞ are the values of the relaxation time and conductivity in the high temperature limit, B is an empirical parameter characteristic of the material accounting for the deviation of linearity (roughly B is lower with the more curve dependence), and T_0 is the Vogel temperature.

The crossover frequency can be used[32] to derive the attempt rate, $\omega_e = 1/\tau_e = (2\pi f_e)$, of the charge carriers to overcame the highest energy barrier that enters in the expression of conductivity contribution in bulk proposed by Dyre[33,34]

$$\sigma^*(\omega) = \sigma_\infty\left(\frac{i\omega\tau_e}{\ln(1 + i\omega\tau_e)}\right) \quad (4)$$

The underlying approach describes the charge transport mechanism as the hopping of charge carriers in a random spatially varying potential landscape; unlike crystals, the potential energy landscape experienced by an ion in a disordered solid is irregular and contains a distribution of depths and barrier heights (schematic representation in ref 23). Basically, the transport process is governed by the ability of charge carriers to overcome the randomly distributed barriers. On short time scales, only the smallest barriers are surmounted, but as time passes, higher and higher barriers are surmounted, and eventually the highest barriers are overcome achieving an infinite cluster of hopping sites that determines the onset of dc conductivity.The frequency f_e, which characterizes this onset of the dc conductivity, is related to it by the empirical relationship known as the Barton−Nakajima−Namikawa (BNN) relationship, $\sigma_0 - 1/\tau_e$ (ref 18 and references therein).

Therefore, similar temperature dependencies for σ_0 and τ_e^{-1} are expected. In figure 5a, the $-\log(\tau_e)$ plot against the reciprocal of temperature was included for all materials, running parallel to the VFT-like temperature dependence of $\sigma_0(T)$. Table 2 presents the estimated parameters of the VFT fit to the $\sigma_0(T)$ and $\tau_e(T)$, where it can be seen the similarity between the B and T_0 parameters obtained from both kind of representations, indicating the parallelism of $\sigma_0(T)$ and $\tau_e(T)$ for all materials. To analyze better the origin of such dependence, the log $\sigma_0(T)$ is represented versus $-\log \tau_e(T)$ in the inset of Figure 5a, this proves that the BNN relationship holds in the studied frequency/temperature range for the four materials as reported for a variety of ion conducting disordered systems.[13,32,35,36]

Figure 5b shows the plot of the normalized conductivity for the value measured at the glass transition temperature, σ_{Tg}, of each system and scaled to T_g. From this plot, it is possible to conclude that relative similar temperature dependencies are observed for the different systems. However, the plots do not follow in a single chart as observed for a series of ionic liquids (inset of Figure 2a in ref 37). The temperature dependence of $BMIMDCA_{1.9\%water}$ conductivity exhibits a relatively higher

Table 2. Fit Parameters Obtained According to the VFT Law for the Conductivity (eq 3b) and the Relaxation Times (eq 3a)[a]

	VFT fit parameters of σ_0[b]			VFT fit parameters of τ_e[c]		
sample	σ_∞ (S cm^{-1})	B (K)	T_0 (K)	τ_∞ (s)	B (K)	T_0 (K)
$BMIMDCA_{1.9\%water}$	37 ± 21	1167 ± 91	136 ± 2	(2.2 ± 0.3) × 10^{-14}	1048 ± 346	136 ± 9
$BMIMDCA_{6.6\%water}$	229 ± 100	1328 ± 58	127 ± 1	(1.3 ± 1.2) × 10^{-16}	1610 ± 374	120 ± 4
ion jelly (IJ3)	59 ± 15	1375 ± 39	128 ± 1	(4.0 ± 2.7) × 10^{-14}	1224 ± 156	130 ± 4
ion jelly (IJ1)	376 ± 116	2453 ± 76	133 ± 1	(1.2 ± 0.6) × 10^{-15}	2508 ± 154	130 ± 3

[a]The uncertainties are the statistical errors given by the fitting program. For each material, the similarity between B and T_0 estimated through $\sigma_0(T)$ and $\tau_e(T)$ indicates a parallelism between these two quantities (see text for details). [b]According to the VFT law for conductivity. [c]According to the VFT law for relaxation time.

dx.doi.org/10.1021/jp2108768 | J. Phys. Chem. B 2012, 116, 2664−2676

curvature, meaning that its conductivity changes more with the temperature while approaching T_g. This can be due to the temperature evolution of the segmental motion to which the conductivity seems to be correlated with (as it will be demonstrated on the last section), and it is usually quantified by the fragility index; this quantity measures the degree of deviation from Arrhenius-type temperature dependence near T_g,[38] but its analysis and determination is out of the scope of this article.

In a few words to finalize this section, the dc conductivity of IJ3 follows closely the behavior of BMIMDCA. At a fixed temperature, the ionic liquid with the highest water amount, $BMIMDCA_{6.6\%water}$, exhibits the highest conductivity, while IJ1 presents the lowest values highly determined by its high glass transition temperature.

3.2.2. Transport Properties. It was previously demonstrated[13] how the BNN relationship, which is followed by these systems as shown in the previous section, can be used to separate the mobility, μ, and the effective number density, n, of charge carriers from σ_0 obtained from the dielectric measurements

$$\sigma_0 = nq\mu \tag{5a}$$

This allows relating dc conductivity and the diffusion coefficient of migrating charges, D, considering the Nernst−Einstein equation

$$\mu = \frac{qD}{k_B T} \tag{5b}$$

as

$$\sigma_0 = \frac{nq^2}{k_B T} D \tag{5c}$$

where q is the elementary charge of an electron, k_B the Boltzmann constant.

By applying the fluctuation−dissipation theorem, Dyre et al.[23] proposed the following expression to account for the relationship between σ_0 and n:

$$\sigma_0 = \frac{nq^2}{6k_B T} \frac{\langle \Delta r^2(t^*) \rangle}{\gamma H} \nu_{cross} \tag{6}$$

where $\langle \Delta r^2(t^*) \rangle$ is the mean-square displacement that is of the order of the distance that a particle can jump when diffusing in a time $t^* = 1/\nu_{cross}$ ($\nu_{cross} = \omega_{cross}/2\pi$), assuming similar jump rates for all ions, and $\gamma \approx 2$ is a numerical factor reflecting the conductivity spectrum at the onset of ac conduction and H is an in principle time-scale-dependent Haven ratio,[35] which accounts for cross correlations between the movements of different types of ions that for ionic liquids can be approximated to 1.5.[39] (see details on the deduction of the equation in ref 23). The factor 6 in eq 6 comes from $2d$ where d is the number of dimensions of the particle trajectory in the absence of electrical field; therefore, $d = 3$ since a three-dimensional motion occurs in this type of disordered material.

Equations 6 and 5c give

$$D = \frac{\langle \Delta r^2(t^*) \rangle}{6\gamma} \nu_{cross} \tag{7}$$

Since the tested systems are constituted by both cations and anions, the overall diffusion coefficient, obtained from dielectric data, can be decomposed to its individual contributions, i.e., D_+ and D_- diffusion coefficients, and therefore, eq 5c can be rewritten as

$$\sigma_0 = \frac{q^2}{6k_B TH}(n_+ D_+ + n_- D_-) \tag{8}$$

From eqs 7 and 8 and by considering that the number density of cations equals the number density of anions, i.e., $n_+ = n_- = n$, we obtain

$$\sigma_0 = \frac{q^2 n}{k_B T} \frac{\nu_{cross}}{6\gamma H} (\langle \Delta r_+^2(t^*) \rangle + \langle \Delta r_-^2(t^*) \rangle) \tag{9}$$

meaning that

$$D_+ = \frac{\langle \Delta r_+^2(t^*) \rangle}{6\gamma} \nu_{cross} \tag{10a}$$

and

$$D_- = \frac{\langle \Delta r_-^2(t^*) \rangle}{6\gamma} \nu_{cross} \tag{10b}$$

where $\langle \Delta r_+^2(t^*) \rangle$ and $\langle \Delta r_-^2(t^*) \rangle$ are the mean-square displacements for the cation and anion, respectively.

An estimate for the mean-square displacement $\langle \Delta r^2(t^*) \rangle$ is to take the square of the van der Waals (vdW) diameter.[40] The vdW value used for BMIM was the one reported in the literature, 0.66 nm.[39] This value is in reasonable agreement with the value of 0.76 nm estimated by using an Hartree−Fock ab initio method provided by a commercially available software;[41] therefore, the vdW diameter estimated by using Spartan[41] for the DCA anion (0.424 nm) was adopted since no value is provide in the literature, as far as we know.

Taking the vdW diameters, the individual diffusion coefficients were estimated from eqs 10a and 10b. The mobility, μ, was then readily determined (eq 5b by taking $D = D_+ + D_-$). In Figure 6, the obtained D_+ and D_- diffusion coefficients (Figure 6a) and μ (Figure 6b) are displayed for $BMIMDCA_{1.9\%water}$ and $BMIMDCA_{6.6\%water}$ and both ion jellies. The estimated self-diffusion coefficients of the cation are slightly higher than those of the anion as generally observed (see ref 39 and references therein), being a consequence of a higher vdW diameter of the former.

Figure 6c includes the cation diffusion coefficients determined from PFG NMR measurements for $BMIMDCA_{6.6\%water}$ and IJ3, the ion jelly containing the same water content; because of the absence of protons or high sensitive NMR nuclei in the anion structure, its diffusion coefficients were not able to be determined by NMR.

For IJ3, it was possible to estimate the cation diffusion coefficients from DRS data over a large temperature range up to the temperature interval covered by PFG NMR measurements. From 213 to 298 K, the crossover frequency was estimated from the dc conductivity values taken at the high frequency plateau through the BNN relationship (stars in Figure 6c). Interesting enough is the fact that the cation diffusion coefficients estimated for IJ3 from dielectric data agree so well with the values directly measured by PGF NMR. Since an average diffusion coefficient is extracted from DRS measurements, this offers a way to validate the deconvolution of this quantity in its individual D_+ and D_- contributions. Concerning the $BMIMDCA_{6.6\%water}$, it was not possible to obtain either crossover frequency or dc conductivity values in the high temperature range due to the influence of electrical anomalies affecting mainly the measurements at the highest

dx.doi.org/10.1021/jp2108768 | J. Phys. Chem. B 2012, 116, 2664−2676

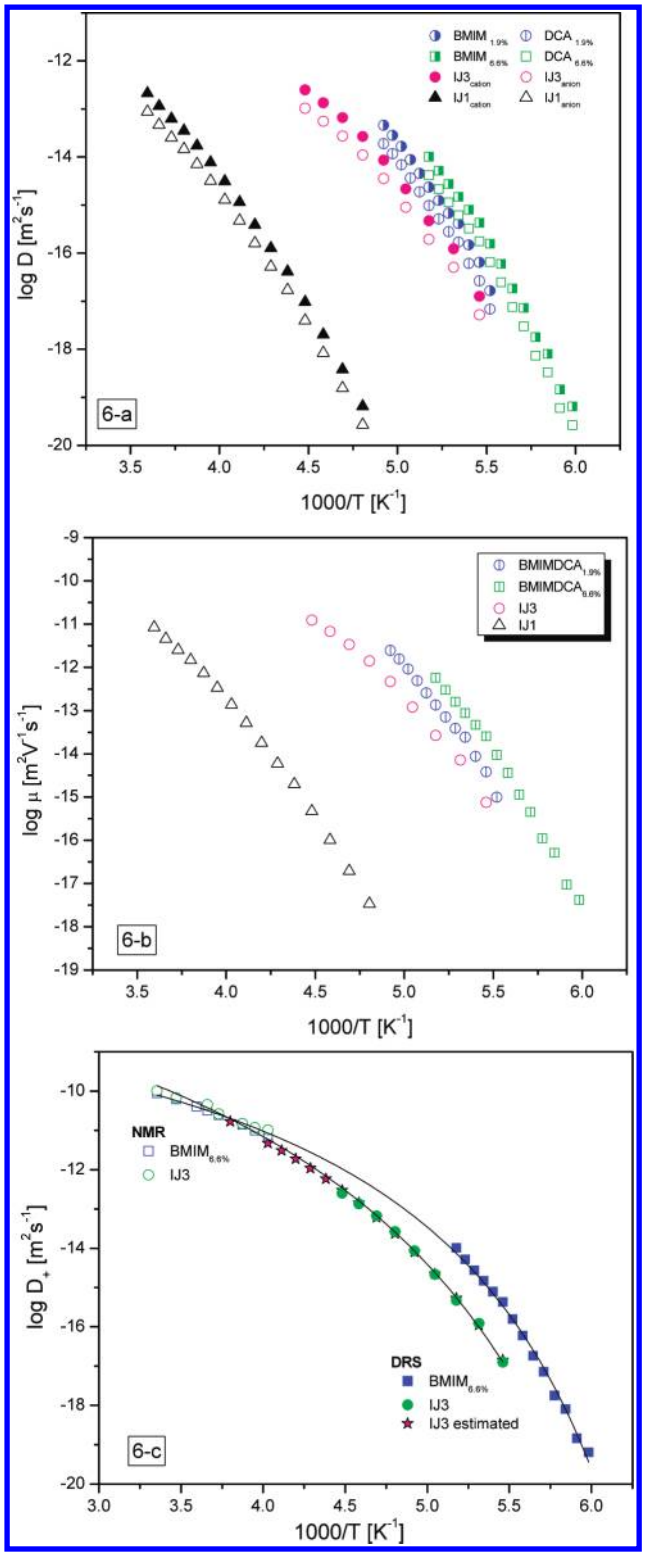

Figure 6. Thermal activation plot for (a) diffusion coefficients of BMIM (cation) and DCA (anion) (eqs 10a and 10b), replacing the mean-square displacement by the vdW diameters, and (b) mobilities, μ, (eq 5b) by taking $D = D_+ + D_-$ for the four materials. (c) Values of the cation diffusion coefficients (D_+) determined from PFG NMR and the VFT fit (solid lines); data represented by stars for IJ3 were estimated also through eq 10a but using the BNN relationship to obtain the crossover frequency from σ_0 (see text).

frequencies as mentioned before. However, a single VFT equation describes both DRS and PFG NMR data.

Before a more detailed analysis, it becomes clear from the plot of the mobility that the nonlinear temperature dependence of conductivity was found to be originated by a VFT behavior of the mobility as found in related materials.[13,26,32]

From the comparison of the transport properties of the ionic liquid with two different water contents, it becomes obvious that water enhances the mobility and increases the value of the ionic diffusion coefficients. The influence of water on the transport properties of several ionic liquids was recently investigated by Spohr and Patey[42] by molecular dynamical simulations that conclude that the dominant effect of water is dynamical in origin. For room temperature IL−water mixtures for which the ion size disparity is not too large (as in the actual IL), it was demonstrated that the lighter water molecules tend to displace much heavier counterions from the ion coordination shells, which reduces caging and increases the diffusivity, leading to higher conductivities and lower viscosities. The results here reported corroborate their conclusions as found also for another ionic liquid (*N*,*N*-diethyl-*N*-methylammoniumtriflate), where it was observed that water facilitates the translational motion of both ions increasing mobility.[43] Moreover, water molecules weaken the contact ion pair since it shields the electrostatic attractions between ions, promoting ion dissociation.[43]

The diffusion coefficients and mobility of charge carriers in IJ3 are close to those of the bulk BMIMDCA. This means that the solid-like material retains a similar ability for charge transport as the ionic liquid. As observed earlier, the gelatin conductivity (even containing a large water amount, 22%) is rather low compared with IJ3 (remember Figure 3). Nevertheless, in IJ3, the gelatin matrix should promote charge separation in large charge clusters, which are known to exist in ILs[44−46]increasing the number of charge carriers resulting in a material with conductivity and mobility comparable to those of the pure IL. The same is not true in IJ1. This is probably due to a rather low ratio BMIMDCA/gelatin, pointing to the existence of a critical composition, which leads to those properties. The difference in the temperature range where these quantities are able to be estimated is determined by the glass transition temperature that, as above-reported, is nearly the same for IJ3 and BMIMDCA and ∼30 K higher for IJ1.

Moreover, it is relevant to observe that the diffusion coefficients at higher temperatures, including room temperature, as measured by PFG NMR, are the same for IJ3 and $BMIMDCA_{6.6\%water}$. Therefore, the presence of the gelatin matrix does not impair the diffusion of the IL ions.

Summarizing this section on transport properties, it was observed for the 4 systems here investigated that the mobility and diffusion coefficients follow a VFT like temperature dependence. Water enhances ion mobility in the bulk ionic liquid; however, in the ion jelly materials, the gelatin amount is significant in determining the transport properties since the composite having the higher water content (IJ1) exhibits the lower diffusion coefficients and mobility. Therefore, a critical composition IL/gelatin should exist above which a self-supported material can exhibit ionic liquid-like properties as found here for IJ3.

3.2.3. Analysis of Real Permittivity ε'. The effect of electrode and interfacial polarization can be also analyzed through the real permittivity spectra, $\varepsilon'(\omega)$, that, oppositely to the dielectric loss, is insensitive to pure dc conductivity; the extremely high values of conductivity made impossible the analysis of any relaxation process including segmental mobility through ε'' data. $\varepsilon'(\omega)$ presents a multimodal character, and therefore, a sum of HN equations (eq 1) was used to fit the raw data. An adequate simulation of the experimental data was only possible

dx.doi.org/10.1021/jp2108768 | J. Phys. Chem. B 2012, 116, 2664−2676

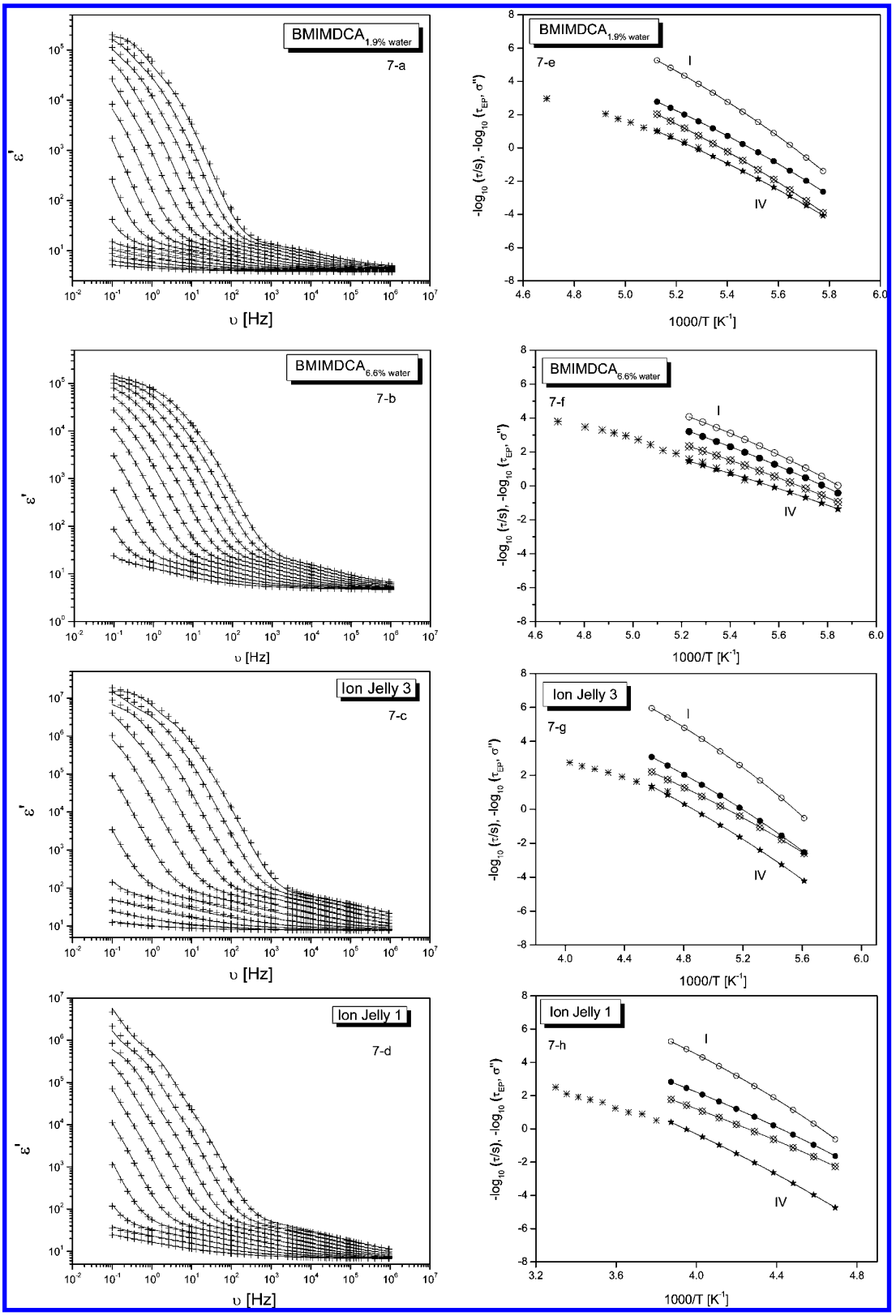

Figure 7. (a–d) Real permittivity spectra, ε', of $BMIMDCA_{1.9\%water}$, $BMIMDCA_{6.6\%water}$, and both ion jellies; the solid lines are the overall fit of a sum of four individual HN functions to the raw data. (e–h) Respective relaxation maps are presented (solid lines are the VFT fit). The asterisks in the relaxation maps are the relaxation times taken from the maximum of $\sigma''(\omega)$ in excellent agreement for all systems with the values estimated from the fit to process IV. Note a different scale in the X axis for IJ1 due to its higher glass transition temperature.

considering four individual processes (designated from I to IV in decreasing order of frequency at the same T). Figure 7a–d shows the obtained result as solid lines illustrating how well data were described by the fit.

dx.doi.org/10.1021/jp2108768 | J. Phys. Chem. B 2012, 116, 2664–2676

In Figure 7e–h, the relaxation maps for all considered processes are displayed. The temperature dependence of the maximum observed in $\sigma''(\omega)$ was included in each relaxation map revealing an excellent agreement with the activation plot of process IV for all systems. This is a way to confirm the accuracy of the fitting procedure and the assignment of this process to electrode polarization.

It should be noted that in spite of expecting a multimodal nature of the dielectric processes due to the simultaneous contribution, in order of increasing frequency, (i) electrode polarization, (ii) interfacial polarization, and (iii) reorientational dipolar motions, it is not straightforward the reason why four processes were needed to simulate the raw data. This can have a real physical meaning due to polarization processes usually found in inhomogeneous materials where internal phase boundaries develop at which charges can be blocked giving rise to different interfacial polarizations of the Maxwell–Wagner–Sillars type;[47] these interfaces in the here-tested materials could be ionic liquid/gelatin, water/ionic liquid, or gelatin/water. Even within the bulk ionic liquid, interfacial polarization can emerge. Indeed, for alkyl-MIM ionic liquids, it was demonstrated by molecular simulation the existence of nanometer-scale structuring with aggregation of the alkyl chains in nonpolar domains, which permeate a tridimensional network of ionic channels formed by anions and by the imidazolium rings of the cations in such a way that microphase segregation exists between polar and nonpolar domains,[44,45]strengthening the existence of interfacial polarization in the pure ionic liquid. However, the need of using four processes could alternatively arise from an inadequacy of a single HN relaxation function to describe the totality of the interfacial processes taking place inside the material. It is not clear up to now what is the actual cause of this behavior.

In Figure 7e–h, it becomes obvious that all considered processes follow VFT dependencies of the respective relaxation times; the VFT parameters are presented in Table 3.

The relaxation process detected at the highest frequencies, i.e., process I, is related to the dipolar relaxation associated with the dynamic glass transition (impossible to analyze from the ε''data, as previously mentioned). From the VFT parameters obtained for process I, it is possible to estimate the glass transition temperature at τ = 100 s,[48]as 171.7 K (−101.5 °C), 164.6 K (−108.6 °C), 172.7 K (−101.0 °C), and 206.6 K(−66.6 °C), respectively, for $BMIMDCA_{1.9\%\ water}$, $BMIMDCA_{6.6\%\ water}$, IJ3, and IJ1. Having in mind that the estimated parameters are being taken from a process that is really weak compared with processes II to IV, the obtained T_g values are in excellent agreement with those determined calorimetrically (see Table 1). Roughly, the magnitude of each process decreases a decade from IV to I, the first having values of the order of 10^6–10^7, while process I has a dielectric strength of the order of hundreds. This is the reason why the frequency dependent real conductivity can be taken as mostly due to subdiffusive transport. The low intensity of the segmental dynamical process compared with conductivity contribution leaves $\sigma'(\omega)$ unaffected, and therefore, meaningful values of crossover frequency, and consequently of τ_σ, were estimated.

3.2.4. Decoupling Index. The VFT dependence obeyed by the relaxation times of process I was also observed for the dc conductivity. This could point to a correlation between the dynamics of the structural relaxation and the ion motion. To test this, the decoupling index, $R_\tau(T_g)$, was determined for each material, which is the ratio of the structural relaxation time

Table 3. VFT Parameters Estimated for Each Process Used in the HN Fit to the ε' Data

	I			II			III			IV		
	τ_∞ (s)	B (K)	T_0 (K)	τ_∞ (s)	B (K)	T_0 (K)	τ_∞ (s)	B (K)	T_0 (K)	τ_∞ (s)	B (K)	T_0 (K)
$BMIMDCA_{1.9\%}$	6.18×10^{-17}	3078.8	107.2	2.32×10^{-19}	3202.2	111.4	9.60×10^{-19}	2953.5	111.0	3.58×10^{-23}	3118.7	116.3
$BMIMDCA_{6.6\%}$	3.45×10^{-13}	2493.2	92.8	1.88×10^{-14}	2349.4	101.7	1.24×10^{-15}	2285.5	106.4	2.06×10^{-16}	2071.7	113.7
ion jelly 3	5.57×10^{-15}	3942.0	85.5	1.527×10^{-14}	3671.1	81	7.40×10^{-17}	3497.6	92.1	2.2×10^{-18}	3031.4	105.7
ion jelly 1	3.69×10^{-14}	4798.1	98.5	9.12×10^{-14}	4447.9	86.9	1.70×10^{-14}	3932.5	102.3	9.69×10^{-18}	3669.9	122.8

dx.doi.org/10.1021/jp2108768 | J. Phys. Chem. B 2012, 116, 2664–2676

to the conductivity relaxation time,[49,50] giving a physical idea of the relationship between the conductivity and structural relaxation processes.[51] This factor conveniently describes the extent to which the ion conducting motions in a given glass can be considered decoupled from the viscous motions of the glassy matrix.[52] An approximate relationship between the logarithm of the decoupling index and the conductivity (in S cm^{-1}) measured at T_g was proposed by Angell[53]

$$\log(R_t(T_g)) = \log(10^{15}\sigma_0(T_g)) \quad (11)$$

giving the orders of magnitude of the mobility of the charge carriers relative to the mobility driven by the segmental dynamics. The σ_0 values obtained at the calorimetric T_g were $\sigma_0(T_g)_{BMIMDCA1.9\%water} = 2 \times 10^{-12}$, $\sigma_0(T_g)_{BMIMDCA6.6\%water} = 8 \times 10^{-12}$, $\sigma_0(T_g)_{IJ3} = 8 \times 10^{-12}$, and $\sigma_0(T_g)_{IJ1} = 3 \times 10^{-13}$ S cm^{-1} given as log decoupling indexes, respectively, 3.3, 3.9, 3.9, and 2.5. In superionic conductors, this value is very large (~7[54] or 9[51]), meaning that the species responsible for conductivity are more mobile 10^7 to 10^9 times than that of the species becoming jammed at the glass transition; it was proposed that the excess mobility was unlikely attributed to any ionic species, instead it should be probably due to the motion of protons themselves.[51] Also, in fast ion-conducting AgI−Ag2O−V_2O_5 glasses, very large values of $R_t(T_g)$ were estimated (from 11 to 14) pointing to a decoupling between the motion of the Ag^+ ion and the matrix.[55] Also in ion gels, the ion transport is found to be decoupled from the segmental motion of the polymers, leading to relatively high ionic conductivities even at their glass transition temperatures (~10^{-7} S cm^{-1}) with $R_t(T_g)$ ≈ 7 in PMMA/[C_2mim][NTf_2] electrolytes.[56]

In the present case, not so high decoupling indexes were estimated meaning by one side that no significant protonic conduction is involved and by other side that segmental motion and conductivity are correlated, which points to a dynamic glass transition assisted hopping mechanism of charge transport as found for related systems.[37]

4. CONCLUSIONS

In the present study, we have characterized the ionic conductivity of BMIMDCA with 1.9 and 6.6% of water content (w/w) and ion jellies with two different ratios of BMIMDCA/gelatin/water, IJ1 (41.1/46.7/12.2) and IJ3 (67.8/25.6/6.6) % (w/w), using dielectric relaxation spectroscopy (DRS) complemented with differential scanning calorimetry and PFG NMR. Through this approach, it was possible to illustrate the impact of gelatin and water on IL physicochemical properties, which are ultimately implicated on ion jelly conductivity.

The calorimetric analysis revealed that all materials undergo glass transition, so they are classified as glass formers. For the ionic liquid BMIMDCA, it was observed that upon hydration, it undergoes a shift of the glass transition toward lower temperatures. The glass transition temperatures for IJs were provided for the first time. Upon dehydration, BMIMDCA undergoes cold crystallization. Contrary, for both IJ1 and IJ3, no crystallization was detected under thermal cycling, which can be seen as a structural advantage of these ion jelly materials.

From dielectric data, it was possible to extract information on the transport properties since it was shown that subdiffusive dynamics govern the conductivity spectra at high frequencies. It was found that ion jelly having the higher IL/gelatin ratio (IJ3) exhibits identical conductive properties to BMIMDCA. In fact, the diffusion and mobility of ionic species are identical on IJ3 and BMIMDCA, meaning that the ionic conductivity is not significantly affected by the presence of gelatin. Nevertheless, an increase of the amount of gelatin lead to a decrease on the ion jelly conductivity showing that there is a critical ratio of IL/gelatin that leads to those properties. For bulk BMIMDCA, it was found that water increases the mobility and the diffusion coefficients, probably due to a weakening of ionic pairs interaction facilitating translational motions. Data treatment was carried out in order to deconvolute the average diffusion coefficients estimated from dielectric data in its individual contributions of cations (D_+) and anions (D_-). The D_+ values thus obtained for BMIMDCA and IJ3 with the same water content (6.6% w/w) revealed mainly for the latter excellent agreement with direct measurements from PFG NMR, obeying the same VFT equation.

A non-Arrhenius temperature dependence of the dc conductivity was observed that is originated by a VFT dependence of mobility in all systems. The VFT dependence of both conductivity and relaxation processes associated with reorientation of dipoles, together with low values of decoupling indexes, point to a correlation between a charge transport mechanism and segmental motion.

A multimodal nature was found in the dynamic behavior as probed by DRS due to simultaneous contribution of dipolar reorientations and interfacial and electrode polarizations. The slowest process was found to be compatible with the electrode polarization process, while the one located at higher frequencies was found to be compatible with the relaxation associated with the dynamic glass transition. From the temperature dependence of relaxation times of the latter process, the glass transition temperatures were estimated in very good agreement with calorimetric data.

Lastly, with the obtained results, we show that ion jelly could be in fact a very promising solution to design novel electrolytes for different electrochemical devices, being much more stable relative to the bulk ionic liquids concerning electrical anomalies that manifest mainly for the IL at high frequencies.

AUTHOR INFORMATION

Corresponding Author

*E-mail: madalena.dionisio@fct.unl.pt.

Notes

The authors declare no competing financial interest.

ACKNOWLEDGMENTS

We thank the financial support to the Fundaçãopara a Ciência e Tecnologia (Portugal) through projects PTDC/CTM/100244/2008 and PTDC/QUI-QUI/098892/2008. T.C. and V. A., respectively, acknowledge the Ph.D. grants SFRH/BD/47088/2008 and SFRH/BD/42322/2007; P.V. acknowledges the postdoc grant SFRH/BPD/41546/2007. The NMR spectrometers are part of the National NMR Network (RNRMN) and are funded by Fundação para a Ciência e Tecnologia.

REFERENCES

(1) Lu, W.; Fadeev, A. G.; Qi, B.; Smela, E.; Mattes, B. R.; Ding, J.; Spinks, G. M.; Mazurkiewicz, J.; Zhou, D.; Wallace, G. G.; et al. *Science* **2002**, *297*, 983−987.

(2) Galinski, M.; Lewandowski, A.; Stepniak, I. *Electrochim. Acta* **2006**, *51*, 5567−5580.

(3) Fernicola, A.; Scrosati, B.; Ohno, H. *Ionics* **2006**, *12*, 95−102.

(4) Ogihara, W.; Washiro, S.; Nakajima, H.; Ohno, H. *Electrochim. Acta* **2006**, *51*, 2614−2619.

(5) Yoshida, Y.; Baba, O.; Saito, G. *J. Phys. Chem. B* **2007**, *111*, 4742−4749.
(6) Leys, J.; Wübbenhorst, M.; Preethy, M. C.; Rajesh, R. T. J.; Glorieux, C.; Nockemann, P.; Thijs, B.; Binnemans, K.; Longuemart, S. *J. Chem. Phys.* **2008**, *128*, 064509−064515.
(7) Winther-Jensen, O.; Vijayaraghavan, R.; Sun, J.; Winther-Jensen, B.; MacFarlane, D. R. *Chem. Commun.* **2009**, *21*, 3041−3043.
(8) He, Y.; Boswell, P. G.; Bulhlmann, P.; Lodge, T. P. *J. Phys. Chem. B* **2007**, *111*, 4645−4652.
(9) Tiyapiboonchaiya, C.; Pringle, J. M.; MacFarlane, D. R.; Forsyth, M.; Sun, J. *Macromol. Chem. Phys.* **2003**, *204*, 2147−2154.
(10) Vidinha, P.; Lourenco, N. M. T.; Pinheiro, C.; Brás, A. R.; Carvalho, T.; Santos-Silva, T.; Mukhopadhyay, A.; Romao, M. J.; Parola, J.; Dionisio, M.; et al. *Chem. Commun.* **2008**, *44*, 5842−5844.
(11) MacFarlane, D. R.; Golding, J.; Forsyth, S.; Forsyth, M.; Deacon, G. B. *Chem. Commun.* **2001**, *16*, 1430−1431.
(12) Aliaga, C.; Baldelli, S. *J. Phys. Chem. B* **2007**, *111*, 9733−9740.
(13) Sangoro, J. R.; Serghei, A.; Naumov, S.; Galvosas, P.; Kärger, J.; Wespe, C.; Bordusa, F.; Kremer, F. *Phys. Rev. E* **2008**, *77*, 051202−051205.
(14) Fredlake, C. P.; Crosthwaite, J. M.; Hert, D. G.; Aki, S. N. V. K.; Brennecke, J. F. *J. Chem. Eng. Data* **2004**, *49*, 954−964.
(15) Havriliak, S.; Negami, S. *Polymer* **1967**, *8*, 161−210. Havriliak, S.; Negami, S. *J. Polym. Sci. Part C: Polym. Symp.* **1966**, *14*, 99−117.
(16) Wu, D.; Chen, A.; Johnson, C. S. Jr. *J. Magn. Reson.* **1995**, *A115*, 260−264.
(17) Troshenkova, S. V.; Sashina, E. S.; Novoselov, N. P.; Arndt, K.-F.; Jankowsky, S. *Russ. J. Gen. Chem.* **2010**, *80*, 106−111.
(18) Kremer, F.; Rozanski, S. A.The Dielectric Properties of Semiconducting Disordered Materials. In *Broadband Dielectric Spectroscopy*; Kremer, F., Schonhals, A., Eds.; Springer-Verlag: Berlin, Germany, 2003; Chapter 12.
(19) Neagu, E.; Pissis, P.; Apekis, L.; Gomez Ribelles, J. L. *J. Phys. D: Appl. Phys.* **1997**, *30*, 1551−1560.
(20) Sun, M.; Pejanović, S.; Mijović, J. *Macromolecules* **2005**, *38*, 9854−9864.
(21) Lu, H.; Zhang, X.; Zhang, H. *J. Appl. Phys.* **2006**, *100*, 054104−054110.
(22) Jonscher, A. K. *Nature* **1977**, *267*, 673−679.
(23) Dyre, J. C.; Maass, P.; Roling, B.; Sidebottom, D. L. *Rep. Prog. Phys.* **2009**, *72*, 046501−046515.
(24) Sangoro, J. R.; Iacob, C.; Naumov, S.; Valiullin, R.; Rexhausen, H.; Hunger, J.; Buchner, R.; Strehmel, V.; Kärger, J.; Kremer, F. *Soft Matter* **2011**, *7*, 1678−1681.
(25) Viciosa, M. T.; Dionísio, M.; GómezRibelles, J. L. *Polymer* **2011**, *52*, 1944−1953.
(26) Iacob, C.; Sangoro, J. R.; Serghei, A.; Naumov, S.; Korth, Y.; Kärger, J.; Friedrich, C.; Kremer, F. *J. Chem. Phys.* **2008**, *129*, 234511−234515.
(27) Vogel, H. *Phys. Z.* **1921**, *22*, 645−646.
(28) Fulcher, G. S. *J. Am. Ceram. Soc.* **1925**, *8*, 339−355.
(29) Tammann, G.; Hesse, W. *Z. Anorg. Allg. Chem.* **1926**, *156*, 245−257.
(30) Stoppa, A.; Zech, O.; Kunz, W.; Buchne, R. *J. Chem. Eng. Data* **2010**, *55*, 1768−1773.
(31) Ito, N.; Huang, W.; Richert, R. *J. Phys. Chem. B* **2006**, *110*, 4371−4377.
(32) Sangoro, J.; Iacob, C.; Serghei, A.; Naumov, S.; Galvosas, P.; Kärger, J.; Wespe, C.; Bordusa, F.; Stoppa, A.; Hunger, J.; et al. *J. Chem. Phys.* **2008**, *128*, 214509−214513.
(33) Dyre, J. C. *J. Phys. C: Solid State Phys.* **1986**, *19*, 5655−5664.
(34) Dyre, J. C. *J. Appl. Phys.* **1988**, *64*, 2456−2468.
(35) Roling, B.; Martiny, C.; Murugavel, S. *Phys. Rev. Lett.* **2001**, *87*, 085901−085904.
(36) Dyre, J. C.; Schrder, T. B. *Rev. Mod. Phys.* **2000**, *72*, 873−892.
(37) Sangoro, J. R.; Iacob, C.; Serghei, A.; Friedrich, C.; Kremer, F. *Phys. Chem. Chem. Phys.* **2009**, *11*, 913−916.
(38) Böhmer, R.; Ngai, K. L.; Angell, C. A.; Plazek, D. J. *J. Chem. Phys.* **1993**, *99*, 4201−4209.
(39) Frömling, T.; Kunze, M.; Schönhoff, M.; Sundermeyer, J.; Roling, B. *J. Phys. Chem. B* **2008**, *112*, 12985−12990.
(40) In ions, the Pauling diameter is often taken as an estimate of the mean square displacement (as mentioned in ref 26), while the vdW diameter refers to neutral atoms/molecules; however, ions in ionic liquids interact via both electrostatic interactions and vdW interactions, so Pauling diameter and vdW diameter can be used indifferently. Moreover, if we compare the assumption of vdW diameter with the equation generally used in the literature where the mean jump length can be defined by the Einstein−Smoluchowski equation as $\langle\lambda^2\rangle = D6\tau$ with $\tau \approx 1/\omega_{cross}$, its value is related with the mean square displacement, as $\lambda = d\mathrm{vdW}/(2\pi)^{1/2}$, which for a van der Waals diameter of 0.66 nm, taken here for the BMIM cation, gives a value of 0.26 nm in excellent accordance with the values estimated for a series of alkyl-3-methyl imidazoliumcations (ref 24).
(41) *Spartan Student*, V4.1.2; Wavefunction Inc.: Irvine, CA.
(42) Spohr, H. V.; Patey, G. N. *J. Chem. Phys.* **2010**, *132*, 234510−234512.
(43) Chang, T. M.; Dang, L. X.; Devanathan, R.; Dupuis, M. *J. Phys. Chem. A* **2010**, *114*, 12764−12774.
(44) Canongia Lopes, J. N. A.; Pádua, A. A. H. *J. Phys. Chem. B* **2006**, *110*, 3330−3335.
(45) Canongia Lopes, J. N.; Costa Gomes, M. F.; Pádua, A. A. H. *J. Phys. Chem. B* **2006**, *110*, 16816−16818.
(46) Triolo, A.; Russina, O.; Bleif, H.-J.; Di Cola, E. *J. Phys. Chem. B* **2007**, *111*, 4641−4644.
(47) Steeman, P. A. M.; van Turnhout, J. Dielectric Properties in Inhomogeneous Media. In *Broadband Dielectric Spectroscopy*; Kremer, F., Schönhals, A., Eds.; Springer-Verlag: Berlin, Germany, 2003.
(48) Richert, R.; Blumen, A., Eds. *Disorder Effects on Relaxational Processes*; Springer: Berlin, Germany, 1994.
(49) Moynihan, C. T.; Balitactac, N.; Boone, L.; Litovitz, T. A. *J. Chem. Phys.* **1971**, *55*, 3013−3019.
(50) Angell, C. A. *Solid State Ionics* **1983**, *9/10*, 3−16.
(51) Mizuno, F.; Belieres, J. P.; Kuwata, N.; Pradel, A.; Ribes, M.; Angell, C. A. *J. Non-Cryst. Solids* **2006**, *352*, 5147−5155.
(52) Ngai, K. L. *J. Phys. IV* **1992**, *2* (C2), 61−73.
(53) Angell, C. A. *Annu. Rev. Phys. Chem.* **1992**, *43*, 693−717.
(54) Sangoro, J. R.; Turky, G.; Abdel Rehim, M.; Iacob, C.; Naumov, S.; Ghoneim, A.; Kärger, J.; Kremer, F. *Macromolecules* **2009**, *42*, 1648−1651.
(55) Bhattacharya, S.; Ghosh, A. *Solid State Ionics* **2003**, *161*, 61−65.
(56) Ueki, T.; Watanabe, M. *Macromolecules* **2008**, *41*, 3739−3749.